

# Numerical Modeling of the Circulation of Wind-Driven Sediment Plumes In Large Lakes

A Thesis SUBMITTED TO THE FACULTY OF THE  
UNIVERSITY OF MINNESOTA BY

**Clay Carufel**

IN PARTIAL FULFILLMENT OF THE REQUIREMENTS FOR  
THE DEGREE OF MASTER OF SCIENCE

**Dr. Jay Austin**

February 2020



# Acknowledgements

I would like to acknowledge:

- My advisor: Dr. Jay Austin
- My thesis defense committee: Dr. Sam Kelly, Dr. John Swenson, and Dr. Alec Habig
- Faculty and staff in the physics department at University of Minnesota Duluth
- Friends and other graduate students at UMD
- My girlfriend Ryley
- My family

*This thesis is dedicated to my family*

# Abstract

Strong winds blowing down the axis of southwestern Lake Superior in the springtime can produce a wind-driven sediment plume. The plume has coastal currents in the same direction as the wind stress and a balancing return flow that is driven by a pressure gradient into the open lake. Analytical developments suggest the return flow volume is determined by the wind stress on the channel and basin morphology. An idealized, three-dimensional model was developed in MITgcm to study this relationship. We find the modeled volume transport to be on the same order of magnitude as the analytical approach and to be dependent on wind stress, basin depth, and basin width. Realistic, three-dimensional models of Lake Superior and Lake Huron are developed to understand the relationship between wind stress on the lakes and the circulation driving wind-driven sediment plumes in them. We find that analytical estimates of volume transport are on the same order of magnitude as the realistic models and that the volume transport is linearly related to the wind stress.

# Contents

<b>List of Figures</b>	<b>v</b>
<b>1 Introduction</b>	<b>1</b>
1.1 Literature Review . . . . .	2
1.2 Gaps In Knowledge . . . . .	3
<b>2 Idealized Model</b>	<b>4</b>
2.1 Transport Method . . . . .	5
2.2 Stream Function Method . . . . .	6
2.3 Volume Transport, $Q$ . . . . .	9
2.4 Results . . . . .	10
2.5 Discussion . . . . .	15
<b>3 Realistic Model: Lake Superior</b>	<b>16</b>
3.1 Additional Tests . . . . .	20
3.1.1 Surface Slope Analysis . . . . .	20
3.1.2 Realistic Winds and Dye . . . . .	20
3.2 Results . . . . .	22
3.3 Discussion . . . . .	26
<b>4 Realistic Model: Lake Huron</b>	<b>28</b>
4.1 Results . . . . .	30
4.2 Discussion . . . . .	32
<b>5 Conclusion</b>	<b>33</b>
5.1 Significance to Society . . . . .	33
<b>6 Bibliography</b>	<b>35</b>

# List of Figures

1.1	Wind-driven sediment plumes in the Great Lakes. Images are taken from Modis Today ( <a href="http://ge.ssec.wisc.edu/modis-today/">http://ge.ssec.wisc.edu/modis-today/</a> . The Lake Superior and Lake Huron images were taken in late April 2016 and the Lake Michigan image was taken in October 2011) . . . . .	2
2.1	Visualized transports for the channel . . . . .	6
2.2	Volume flux through a line element. Modified from Khundu (3rd edition). . . . .	8
2.3	Contour plots of the stream function (units of $\text{m}^3\text{s}^{-1}$ ) can be used for visualization of the flow and to calculate $q$ . The symbol $t_0$ indicates the initial time the tracer particle is looked at. Stream function plots are from the idealized model. . . . .	9
2.4	Along-channel velocity with depth at the transect. Units on the colorbar are $\text{ms}^{-1}$ . . . . .	10
2.5	Comparison of numerical model's surface slope in middle of channel on the x-axis and analytical surface slope on the y-axis . . . . .	11
2.6	Time series of $q$ calculated using the transport method . . . . .	12
2.7	Time series of $q$ calculated using the stream function method . . . . .	13
2.8	Total volume moved offshore for varying wind stress. Results from transport and stream function methods are plotted . . . . .	14
2.9	Experimental $Q$ values are plotted against $Q$ predicted by Equation 2.3 . . . . .	14
2.10	Vertical viscosity values output by KPP algorithm in the middle of the channel. The colorbar has units of $\text{m}^2\text{s}^{-1}$ . . . . .	15
3.1	Model bathymetry in meters . . . . .	16
3.2	Northeast winds blowing down the western arm of Lake Superior . . . . .	17
3.3	Transports are investigated along the transect and measured along the new axes . . . . .	18
3.4	Transports are evaluated on the transect line . . . . .	19
3.5	Selection of the zero-crossing points (black stars) in the transport streamfunction field. Units on the colorbar are $\text{m}^3\text{s}^{-1}$ . . . . .	19
3.6	Points on the grid chosen for $\eta$ measurements are marked by black stars. They are approximately 460 km apart. Plotted field is $\eta$ and colorbar has units of meters . . . . .	20
3.7	Wind direction and speed recorded by DULM5 for April 23-29, 2016. $0^\circ$ would indicate a wind from the north . . . . .	21
3.8	Approximate dye input points . . . . .	22

---

3.9	Vertical profile of along-channel velocity at transect. Colorbar has units of $\text{ms}^{-1}$ . . . . .	23
3.10	Time series of $q$ calculated using the transport method. The northeast wind stress is varied. $\tau_0 = 0.1 \text{ Nm}^{-2}$ . . . . .	23
3.11	Experimental $Q$ results using transport and stream function methods	24
3.12	Experimental $Q$ values are plotted against analytical $Q$ . . . . .	24
3.13	Slope of free surface between the points shown in Figure 3.6 and setup at southwestern coast of Lake Superior with varying wind stress . . .	25
3.14	Vertically-integrated dye 1 concentration . . . . .	26
3.15	Vertically-integrated dye 2 concentration . . . . .	26
3.16	Vertical profile of along-channel velocity in return flow . . . . .	27
4.1	(a) Observed sediment plume in Lake Huron develops in the southeastern portion of the basin. (b) Wind data collected from weather station PSCM4 for dates plume was observed on (April 23-29, 2016). $0^\circ$ indicates a wind that blows from the north. . . . .	28
4.2	Model bathymetry in meters . . . . .	29
4.3	The model is forced by wind stress pointing down the southeastern basin . . . . .	29
4.4	Transports are investigated along the transect line . . . . .	30
4.5	Along-channel velocities with depth on transect line. Units on the colorbar are $\text{ms}^{-1}$ . $\tau^{sfc} = 0.1 \text{ Nm}^{-2}$ . . . . .	30
4.6	Time series of $q$ calculated using the transport method with varying wind stress. $\tau_0 = 0.1 \text{ Nm}^{-2}$ . . . . .	31
4.7	Comparison of $Q$ for the three methods . . . . .	31
4.8	Vertical profile of along-channel velocity in return flow . . . . .	32

# Chapter 1

## Introduction

In the springtime, strong storms with northeast winds frequently develop over Lake Superior. Once the storm has passed, residents of Duluth, MN looking out to the water may be met with a striking visual: a large, red stripe up the middle of the lake called a wind-driven sediment plume.

Wind-driven sediment plumes may develop at other times of the year and in parts of the lake with other bottom topographies, but plumes that form in the spring and in a channel like southwestern Lake Superior are studied here. Along with the strong winds mentioned earlier, the water has a uniform density from top to bottom and there is no ice on the water's surface. A channel amenable to the development of the plume will have shallow water near the shore and deeper water in the middle. Additionally, the bottom topography should rise at the end of the channel, most likely the shoreline, acting like a block to water flow.

As the wind blows, a two cell circulation pattern forms with strong coastal jets that move in the direction of the wind stress. The coastal jets are balanced by a return flow in the center of the channel which moves opposite to the wind stress. The return flow is driven by a pressure gradient due to high water on the leeward/shore-end of the channel.

Suspended sediment that was deposited from coastal erosion, riverine inputs, or resuspension of sediment in the channel travels with the return flow and gives the channel its striped appearance as viewed either from the shore or satellite imagery (Fig 1.1).

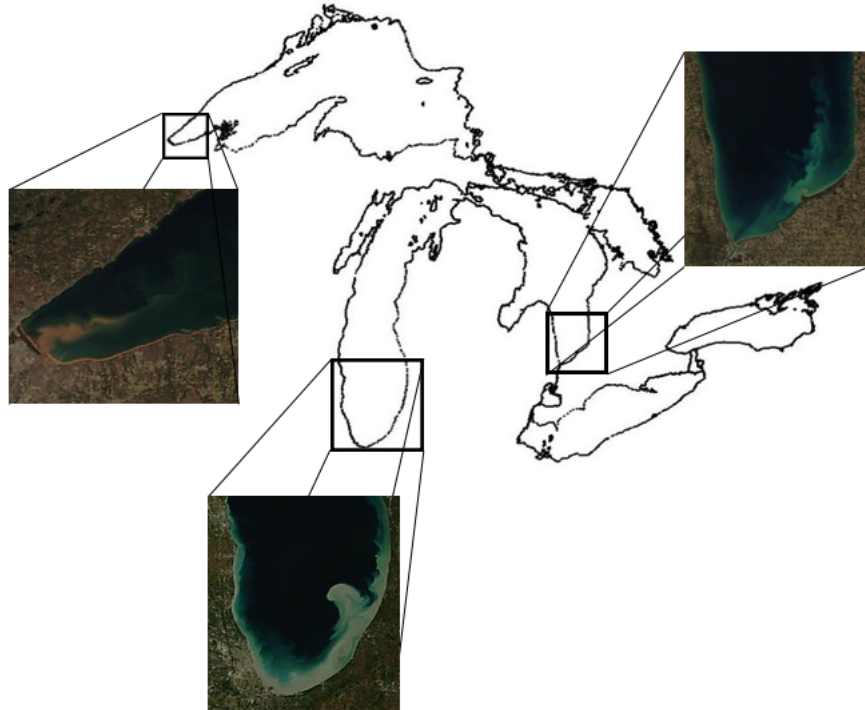


Figure 1.1: Wind-driven sediment plumes in the Great Lakes. Images are taken from Modis Today (<http://ge.ssec.wisc.edu/modis-today/>). The Lake Superior and Lake Huron images were taken in late April 2016 and the Lake Michigan image was taken in October 2011)

McKinney et al. (2019) show that the return flow in a wind-driven sediment plume in Lake Superior is composed of coastal water. Coastal water can be differentiated from the open lake due to the cross-shelf gradient in chemical, biological, and physical constituents. These parameters become concentrated in the coastal area due to the surrounding watershed and hydrodynamic constraints that favor transport that aligns with bathymetry [2]. Due to variations in frequency and intensity of the northeast storms behind Lake Superior's sediment plume, the total volume of water transported offshore from year-to-year varies as well. This source of cross-shelf transport may play a role in the ecological variability of the lake from year-to-year. Cross-shelf transport processes are important as they redistribute dissolved and particulate matter across the gradients, affecting the coastal and pelagic ecosystems [19].

## 1.1 Literature Review

McKinney et al. (2019) analyzed the recurrent wind-driven sediment plume in Lake Superior that forms to the west of the Apostle Islands and that develops when strong winds blow from the northeast in the springtime. The plume was analyzed on a variety of temporal and spatial scales using autonomous vehicles, in-situ profilers, satellite imagery, and an idealized analytical model. The analytical model predicts a linear relationship between the wind stress and the volume of water that is transported offshore in a plume event. The volume of water moved offshore

---

was also estimated by using satellite images of the plume to differentiate between plume-impacted and non-impacted water. The volume flux predicted by the analytical model was compared to estimates made by the satellite image technique for a storm in late April 2016 and both methods predicted the volume of water moved offshore to be on the order of  $10^{10}$  m<sup>3</sup>. The authors analyzed 10 plume events using the satellite image technique and saw strong linear correlation between plume area and volume of water transported offshore with wind stress. The authors hypothesize that since the frequency of the events varies from year to year, the plume may play a role in the interannual variability in the ecosystem of Lake Superior and the plumes themselves act as an important cross-shelf transport mechanism.

The two-cell circulation pattern that forms when winds blow over a channel with unstratified waters in the Great Lakes has been investigated extensively. Rao and Murthy (1970) have studied wind-driven circulation in Lake Ontario during unstratified periods. Utilizing an analytical model with realistic bathymetry they showed that a two-cell circulation pattern forms with strong coastal jets following the wind stress and a weaker return flow that moves opposite to the wind stress.

Csanady (1973) studied wind-driven circulation on the Great Lakes during unstratified periods by using an analytical model with a general elongate lake basin with variable bathymetry. The same two-cell circulation pattern reported by Rao and Murthy (1970) was produced by the model. It was also shown that transports were in the direction of the wind in places where the depth was less than the average basin depth and in directions opposite to the wind where the depth was greater than the average basin depth.

Multiple observational studies (Eadie et al. (1996); Lohrenz et al. (2004); Vanderploeg et al. (2007)) have been carried out on Lake Michigan where a recurrent wind-driven sediment plume develops in the southern end of the lake. It was seen in Eadie et al. (1996) that the plume drives a significant amount of biological activity and contributed approximately 25% of annual sediment to the southern end of the lake in 1996.

## 1.2 Gaps In Knowledge

Understanding the volume of water transported offshore remains an important question related to wind-driven sediment plumes due to the organic matter, sediment, and potential pollutants that are moved to the interior of the lake. McKinney et al.'s linear theory predicts the volume of water moved offshore is linearly related to wind stress on the system, basin depth, and basin width. These dependencies will be investigated further.

The study of wind-driven plumes naturally lends itself to the study of storm surge on Lake Superior. Storm surge takes place when strong winds and changes in atmospheric pressure lead to water levels rising above normal levels [13]. Storm surge on Lake Superior and at the southwest end of it due to a northeast wind in particular remain understudied topics.

To begin to address these gaps, numerical models of the circulation of wind-driven sediment plumes are utilized and presented in the following chapters.

# Chapter 2

## Idealized Model

McKinney et al. (2019) present an analytical model that predicts the volume flux of the return flow,  $q$ , for a plume event in a basin of variable bathymetry

$$q = \int_{y_1}^{y_2} r^{-1} (1 - gH(y)b) \frac{\tau^{sfc}}{\rho} H(y) dy \quad [\text{m}^3\text{s}^{-1}] \quad (2.1)$$

where  $y$  is the cross-channel direction,  $H$  is the depth of the channel, and  $y_1$  and  $y_2$  are two positions of zero-crossings in the along-channel velocity. The value of  $b$  can be solved for using

$$b = \frac{\int_{-L}^L H(y) dy}{g \int_{-L}^L H(y)^2 dy} \quad (2.2)$$

where  $L$  is half the width of the basin and  $g$  is the gravitational acceleration. Using 2.1, the value of  $q$  can be found for the special case of a basin with parabolic bathymetry in the cross-shore direction

$$q = \frac{8}{25\sqrt{5}} \frac{H_0 L \tau^{sfc}}{r \rho} \quad (2.3)$$

where  $L$  is half the width of the channel,  $H_0$  is the max depth of the basin,  $\tau^{sfc}$  is the wind stress,  $r$  is a bottom drag coefficient, and  $\rho$  is the density of the water.

To test the formulation in Equation 2.3 and hence, the more general formulation of Equation 2.1, experiments are carried out using the MITgcm numerical model. MITgcm is a non-hydrostatic and vertical z-level model that has the capabilities to simulate fluid motion in both the the atmosphere and ocean/lakes [11]. Numerical models are an important tool in limnology/oceanography as they serve as a way to experiment with complicated lakes/oceans, to determine optimal locations to place instrumentation, and to test hypotheses. An idealized model is developed with parabolic bathymetry and uniform wind forcing on the system. The wind forcing is always in the along-channel direction.

For all experiments, the horizontal resolution in the  $x$  and  $y$  directions are  $\Delta x$ ,  $\Delta y = 250$  m and the vertical resolution is  $\Delta z = 2$  m. The coastal jets and return flow are well-resolved since their horizontal length scales are multiple kilometers.

---

Eddies in the flow that are smaller than the grid scale act as a path of momentum transfer and should be incorporated into the model. To do this, the Smagorinsky closure scheme is used for the horizontal transfer of momentum of the eddies while the KPP algorithm is employed along the vertical direction. A value of 3 (non-dim.) is chosen for the Smagorinsky harmonic viscosity factor as the MITgcm manual stated this was common practice for oceanic models. A value of  $10^{-3} \text{ m}^2\text{s}^{-1}$  is the background vertical eddy viscosity. A linear bottom drag is chosen for the model with  $r = 5 \times 10^{-4} \text{ m s}^{-1}$  (Beardsley et al., (1977)), consistent with McKinney et al.'s analytical model. The simulation is run for 180 hours in model time.

The model outputs variables at each time and spatial step. The variables include the cross-channel and along-channel components of the velocity field, written as  $u$  and  $v$ , respectively. The  $v$  velocity component is used to measure the magnitude of  $q$  from distinct model runs where either  $\tau^{sf_c}$ ,  $H_0$ , or  $L$  is adjusted while the others are held fixed.  $q$  is estimated via both a transport method and using the transport stream function which are described in the following sections.

## 2.1 Transport Method

Transports are the vertical integrals of  $u$  and  $v$

$$U = \int_{-h}^0 u \, dz \quad \text{and} \quad V = \int_{-h}^0 v \, dz \quad [\text{m}^2\text{s}^{-1}] \quad (2.4)$$

where  $-h$  is the depth at a point in the channel.

The transports are investigated along a transect in the middle of the basin where irregularities in the flow due to channel walls are minimal (Figure 2.1).

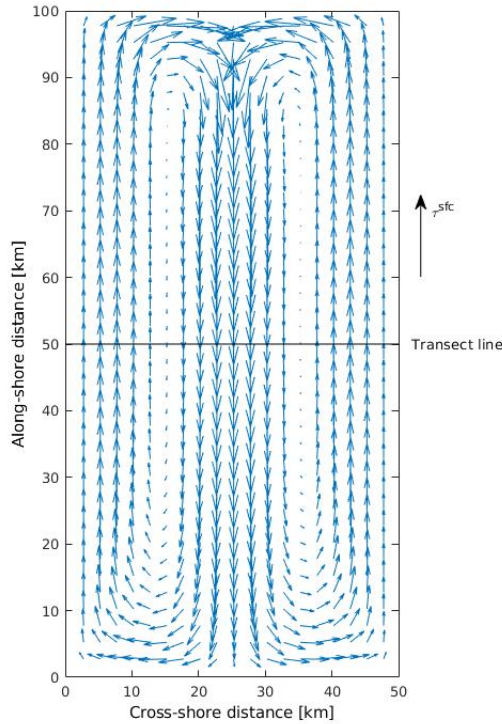


Figure 2.1: Visualized transports for the channel

At each time step, the along-channel transports pointing opposite to the wind stress are found and multiplied by the grid spacing in the cross-channel direction. The sum of these products is then used as a measure of the volumetric flux,  $q$ , across the transect for that time step. A low-pass filter is then used on the  $q$  time series to subtract out basin seiche waves. This allows for a more objective measure of when the system reaches a steady-state. Steady-state is identified as the time where the flow rate is less than one percent of the total flow rate for two consecutive time steps. It is important to identify the steady-state time because the numerical model is compared to the analytical model which is formulated in steady-state.

## 2.2 Stream Function Method

The transport stream function is calculated as a check on the transport method from above. Following the approach given by C.C. Mei [10], the transport stream function can be derived by integrating the continuity equation with a surface,  $z = \eta(x, y, t)$ , boundary condition of

$$w = \frac{\partial \eta}{\partial t} + u \frac{\partial \eta}{\partial x} + v \frac{\partial \eta}{\partial y} \quad (2.5)$$

and on the bottom  $z = -h(x, y)$

$$w = -u \frac{\partial h}{\partial x} - v \frac{\partial h}{\partial y} \quad (2.6)$$

Carrying out the integration

---


$$\begin{aligned}
0 &= \int_{-h}^{\eta} \left( \frac{\partial u}{\partial x} + \frac{\partial v}{\partial y} + \frac{\partial w}{\partial z} \right) dz \\
&= [w]_{-h}^{\eta} + \frac{\partial}{\partial x} \int_{-h}^{\eta} u dz + \frac{\partial}{\partial y} \int_{-h}^{\eta} v dz \\
&\quad + \frac{\partial \eta}{\partial x} u(\eta) - \frac{\partial h}{\partial x} u(-h) - \frac{\partial h}{\partial y} v(-h)
\end{aligned} \tag{2.7}$$

Knowing that  $H = \eta + h$

$$0 = \left( w - u \frac{\partial \eta}{\partial x} \right)_{\eta} - \left( w - u \frac{\partial \eta}{\partial x} \right)_{-h} + \frac{\partial H u}{\partial x} + \frac{\partial H v}{\partial y} \tag{2.8}$$

Plugging in the boundary conditions we are left with

$$\frac{\partial H}{\partial t} + \frac{\partial U}{\partial x} + \frac{\partial V}{\partial y} = 0 \tag{2.9}$$

where  $U$  and  $V$  are transports once again. If the system of interest is in steady-state, the time derivative of  $H$  can be dropped

$$\frac{\partial U}{\partial x} + \frac{\partial V}{\partial y} = 0 \tag{2.10}$$

Equation 2.10 can be satisfied by the introduction of the stream function,  $\psi$

$$U = \frac{\partial \psi}{\partial y} \quad \text{and} \quad V = -\frac{\partial \psi}{\partial x} \tag{2.11}$$

In this case,  $U dy - V dx$  is an exact differential and can be written as

$$d\psi = U dy - V dx \tag{2.12}$$

The stream function can be interpreted in two important ways. If looking at a point of constant  $\psi$ , the left side of equation 2.12 is equal to zero and the equation can be rearranged to obtain

$$\frac{U}{V} = \frac{dx}{dy} \tag{2.13}$$

which is the equation for a streamline. Consequently, lines of constant  $\psi$  are streamlines making them useful for flow visualization.

Following Kundu (3rd edition, pg. 70-71), the flow through the line element  $d\mathbf{x} = (dx, dy)$  in Figure 2.2 is equal to

$$V dx + (-U) dy = -d\psi \tag{2.14}$$

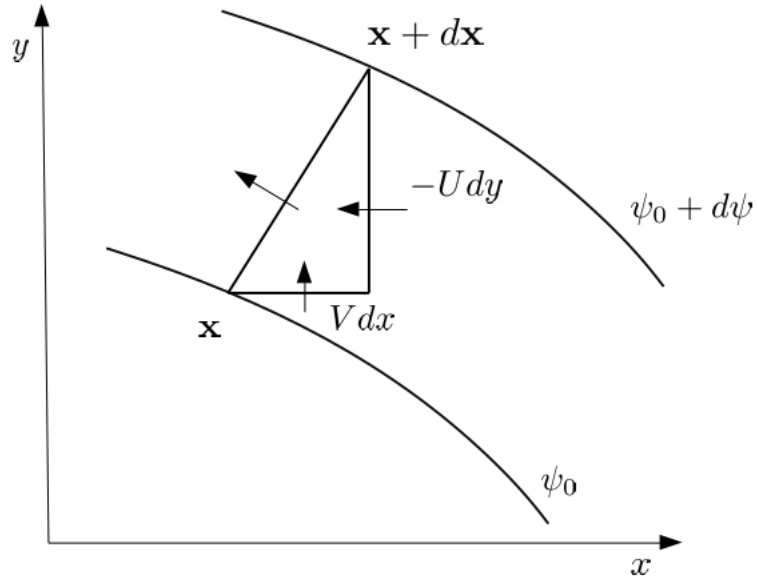


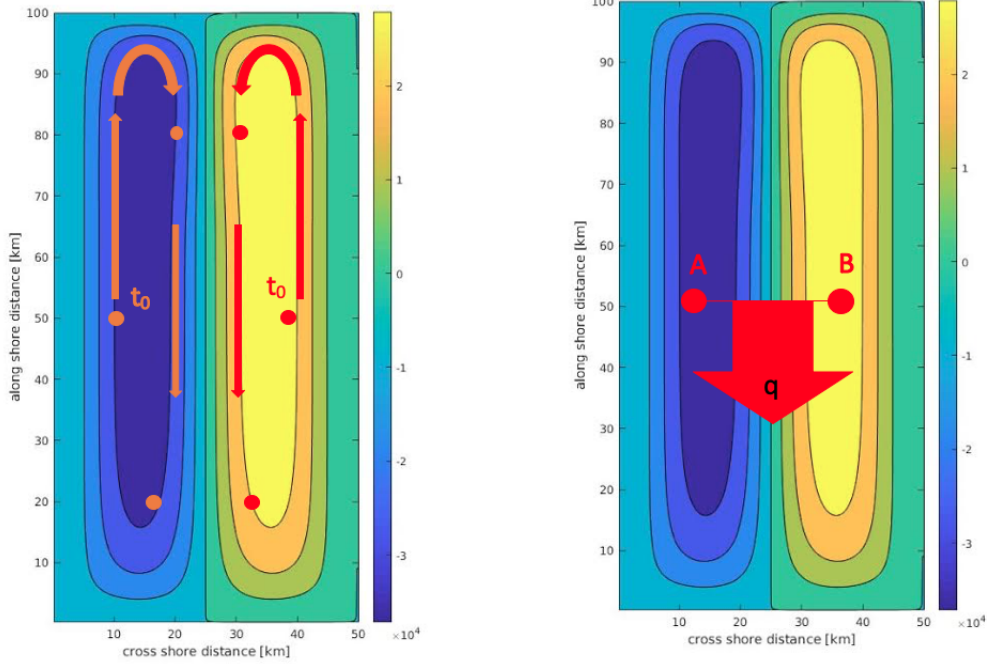
Figure 2.2: Volume flux through a line element. Modified from Khundu (3rd edition).

which shows that the difference in the  $\psi$  value on two streamlines is equal to the volume flux through the line element that connects them since  $\psi_0 - (\psi_0 + d\psi) = -d\psi$ .

Equation 2.12 is integrated to obtain

$$\psi - \psi_0 = \int_A^B (U dy - V dx) \quad (2.15)$$

where  $\psi$  and  $\psi_0$  are the stream function values at the spatial coordinates  $B$  and  $A$ , respectively. Equation 2.15 is path-independent meaning either  $\int_A^B U dy$  or  $-\int_A^B V dx$  can be evaluated numerically to find  $\psi$  at each grid point.



(a) Particles moving along streamlines (b) Volume flux between two points

Figure 2.3: Contour plots of the stream function (units of  $\text{m}^3\text{s}^{-1}$ ) can be used for visualization of the flow and to calculate  $q$ . The symbol  $t_0$  indicates the initial time the tracer particle is looked at. Stream function plots are from the idealized model.

Two zero-crossings in the along-channel component of the transport field are seen by an observer moving along the transect line due to the coastal jets following the wind stress and the return flow moving opposite to it. The zero-crossing locations are used as the boundary of the return flow and the difference in the  $\psi$  values at those points is taken to measure the magnitude of  $q$  at that time step. The  $q$  time series is analyzed in the same way as the transport method to determine when the system reaches a steady-state.

## 2.3 Volume Transport, $Q$

After the flow rate has reached a steady-state,  $q$  is integrated in time to find the total volume transported by the return flow,  $Q$

$$Q = \int_{t_1}^{t_2} q(t) dt \quad [\text{m}^3] \quad (2.16)$$

where  $t_1$  is the time where the system reaches a steady-state and  $t_2$  is the ending time of the model run. Following McKinney et al. (2019) and using Equation 2.1, it's shown that  $Q$  can be written as

$$Q = \int_{t_1}^{t_2} \int_{y_1}^{y_2} r^{-1} (1 - gH(y)b) \frac{\tau^{sfc}(t)}{\rho} H(y) dy dt \quad (2.17)$$

If the wind stress is the only time-dependent variable in Equation 2.17, the equation can be written as

$$Q = \left[ \int_{y_1}^{y_2} r^{-1} (1 - gH(y)b) \frac{H(y)}{\rho} dy \right] I \quad (2.18)$$

where

$$I = \int_{t_1}^{t_2} \tau^{sfc}(t) dt \quad (2.19)$$

is the specific impulse applied to the lake during a wind event. Equation 2.18 predicts that the volume of water moved offshore due to a wind event is then related to basin morphology and both the duration and intensity of the wind event over the lake. Comparing a plume's yearly  $Q$  to other years could support the hypothesis that interannual ecological variability in the part of the lake the plume forms in is connected to  $Q$ .

## 2.4 Results

The idealized model produces the expected features of the plume's circulation, strong coastal currents in the shallower regions of the channel and a compensating return flow in the deeper sections. The coastal jets and return flow extend from the surface of the water column to the bottom with little overlap between the two (Figure 2.4). For the base case model run, the mean experimental return flow velocity was  $0.057 \text{ ms}^{-1}$  while the mean analytical value was  $0.033 \text{ ms}^{-1}$  once the system reached a steady-state.

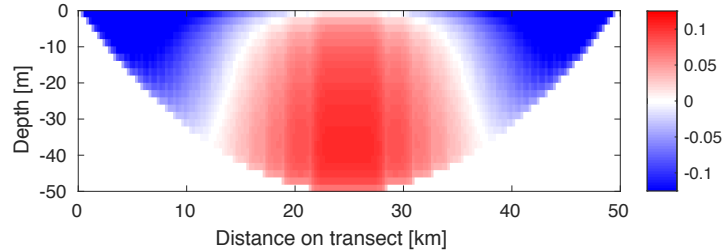


Figure 2.4: Along-channel velocity with depth at the transect. Units on the colorbar are  $\text{ms}^{-1}$ .

Modeled and analytical surface slopes were largely similar but since the modeled surface slope was larger with wind stress it may account for some of the larger modeled return flow velocities (Figure 2.5).

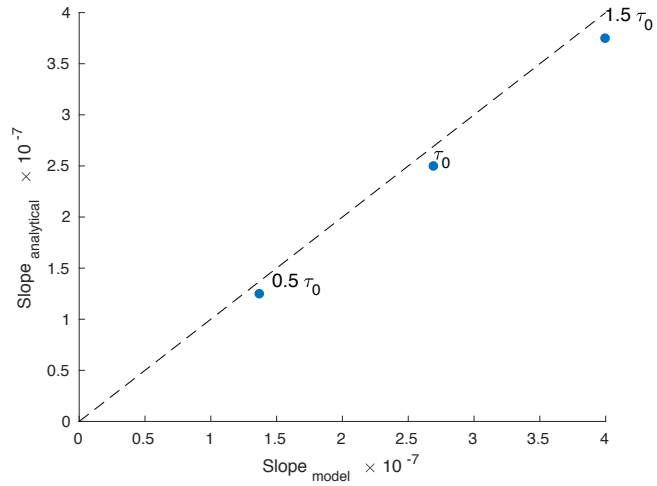
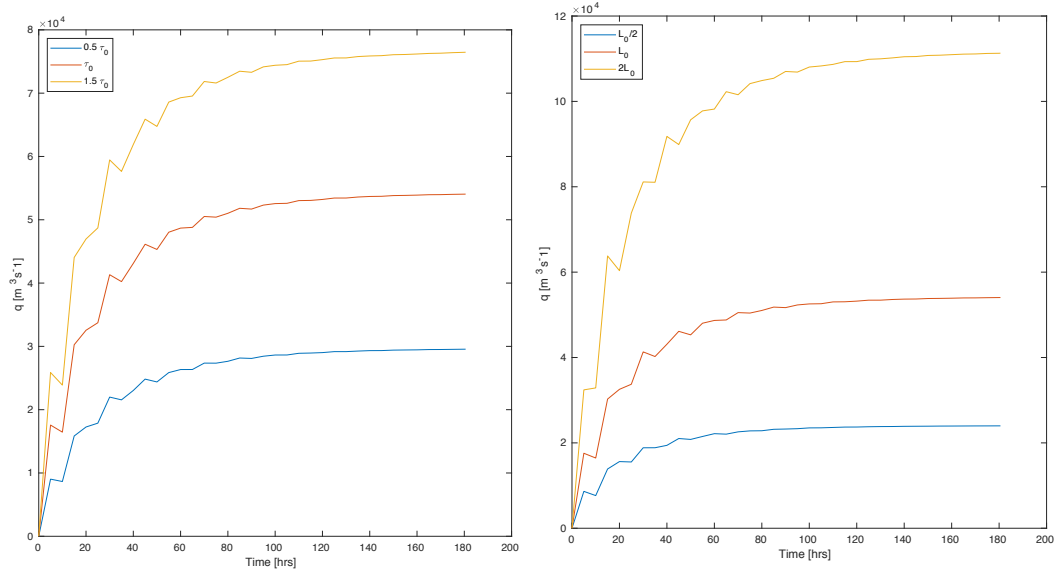
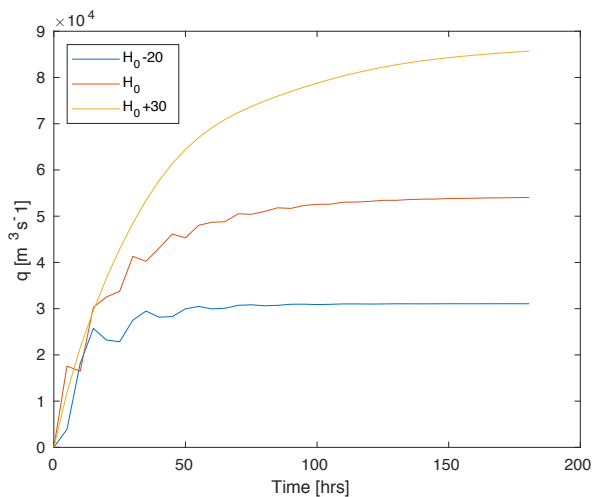


Figure 2.5: Comparison of numerical model’s surface slope in middle of channel on the x-axis and analytical surface slope on the y-axis

The flow rate across the transect was measured in the model as the wind stress on the channel, the width of the basin, and the depth of the basin are varied. Model parameters are varied around a “base case” which is a parabolic channel with a max depth of 50 m, a width of 50 km, and a wind stress on the channel of  $0.1 \text{ Nm}^{-2}$  (Figure 2.6).



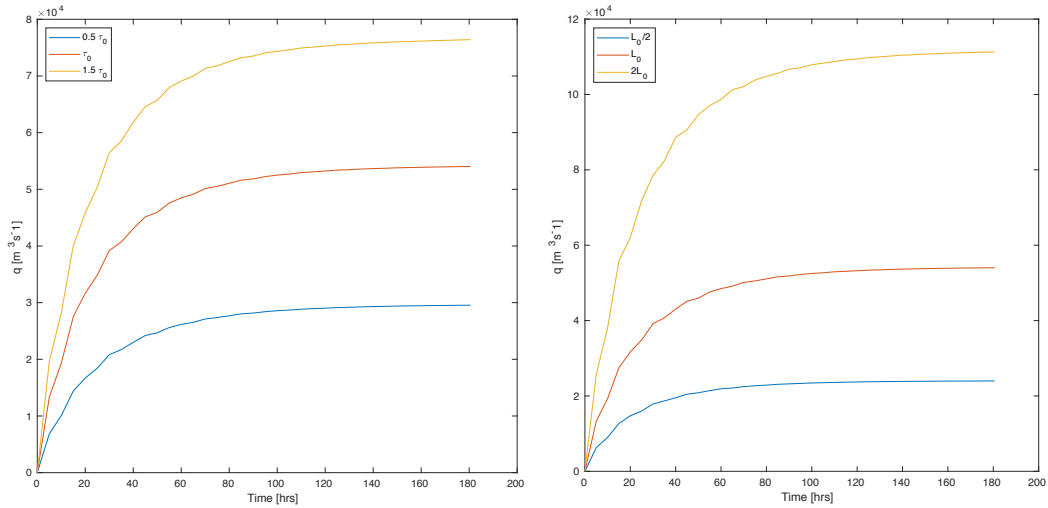
(a) Varying wind stress on channel.  $\tau_0 = 0.1 \text{ Nm}^{-2}$  (b) Varying basin width.  $L_0$  is half the basin width and equal to 25 km



(c) Varying depth of basin.  $H_0 = 50 \text{ m}$

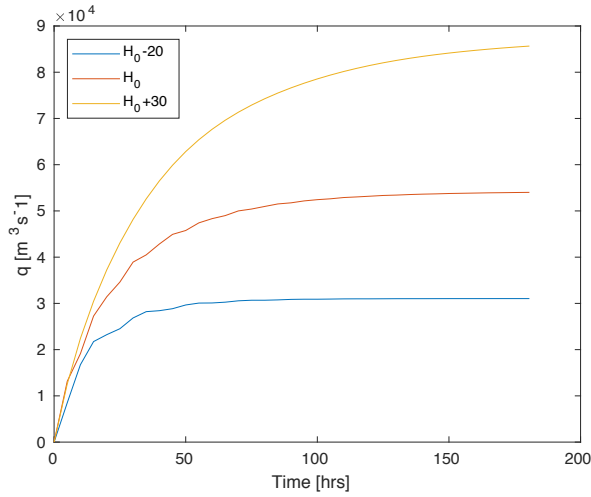
Figure 2.6: Time series of  $q$  calculated using the transport method

A similar time series of the flow rate is plotted where the difference in the stream function is used. The wind stress on the channel, the max depth of the basin, and the width of the basin are varied once again (Figure 2.7).



(a) Varying wind stress on channel

(b) Varying basin width



(c) Varying depth of basin

Figure 2.7: Time series of  $q$  calculated using the stream function method

Figure 2.6 and Figure 2.7 show that for all model runs the flow rate initially increases and then eventually reaches a steady-state. The plots show how the steady-state flow rate changes when the wind stress and basin dimensions are varied. The flow rate curves could be fit with the function  $q = q_{steady} (1 - e^{-at})$  where  $q_{steady}$  is the steady-state flow rate and  $a$  is a decay scale. This is in agreement with Csanady's (1973) analytical investigation of wind-induced motion in lakes where bottom friction is not negligible.

Integration of the flow rates shows that the two experimental methods for determining  $q$  give comparable results for  $Q$  (Figure 2.8). To avoid redundancy, analytical results will primarily be compared to only the transport method going forward.

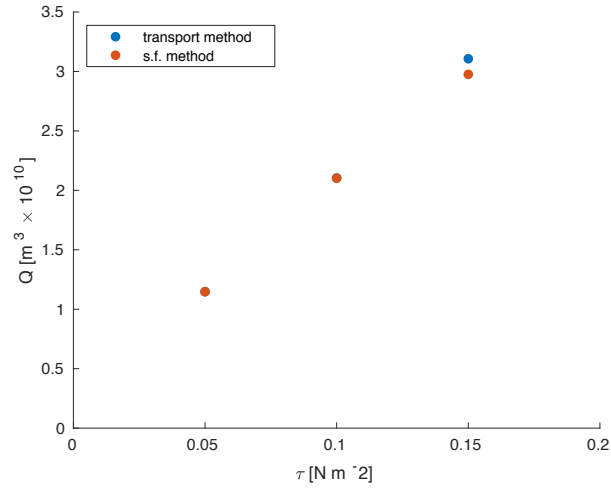
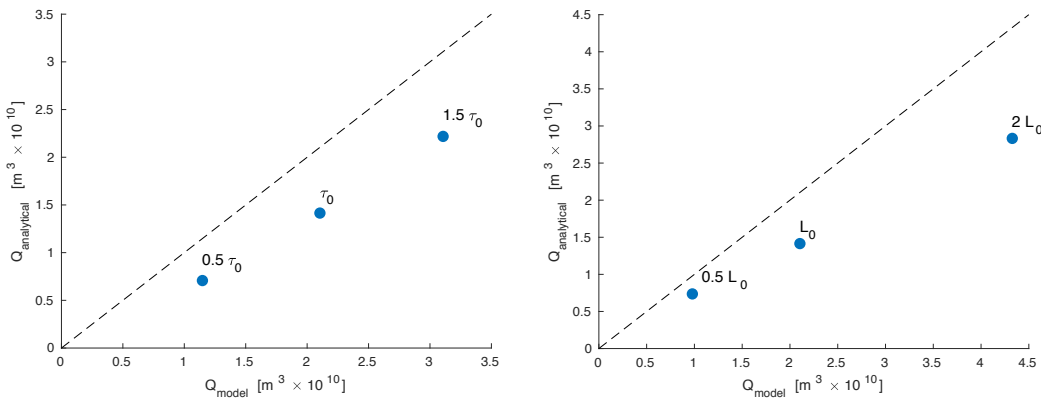


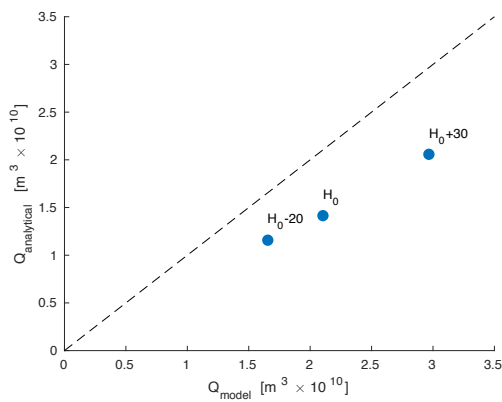
Figure 2.8: Total volume moved offshore for varying wind stress. Results from transport and stream function methods are plotted

Since offshore volume transport is dependent on flow rates, modeled  $Q$  was always larger than the analytical estimate (Figure 2.9).



(a) Varying wind stress on channel

(b) Varying basin width



(c) Varying depth of basin

Figure 2.9: Experimental  $Q$  values are plotted against  $Q$  predicted by Equation 2.3

---

Figure 2.9 shows that like the analytical formulation, experimental  $Q$  varies linearly with changing basin dimensions and wind stress on the channel.

## 2.5 Discussion

In this chapter, an idealized circulation model was used to study the circulation of wind-driven sediment plumes. We showed that like an analytical approach, experimental  $Q$  changed linearly with varying wind stress and basin morphology. The experimental estimates of  $Q$  were always larger than analytical estimates but the two were always on the same order of magnitude.

The free model parameters that could alter the flow rates substantially are the background vertical viscosity and the bottom drag coefficient. Choosing a larger background vertical viscosity or bottom drag coefficient would result in experimental estimates being closer to the analytical estimates. However, the chosen bottom drag coefficient is taken from experiment and so assumed reasonable. As for the background vertical viscosity, it is generally smaller than the vertical viscosity values output by the KPP algorithm (Figure 2.10) so significant changes to these two parameters does not seem required. Ultimately, differences between the analytical solution and three-dimensional model may always arise as the analytical derivation is inviscid and the circulation model is not.

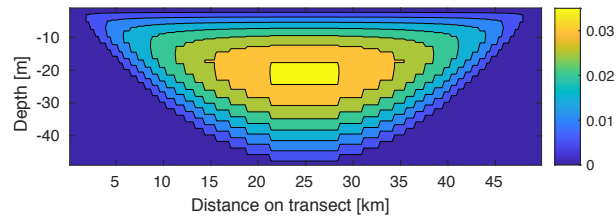


Figure 2.10: Vertical viscosity values output by KPP algorithm in the middle of the channel. The colorbar has units of  $\text{m}^2\text{s}^{-1}$ .

A simple, idealized model was studied in this chapter. In the next one, a more complex case is considered: realistic circulation of Lake Superior.

## Chapter 3

# Realistic Model: Lake Superior

Realistic models aim to be as similar to the real physical system as possible. To this end, a realistic model of Lake Superior is developed and simulated using the ROMS numerical model. An orthogonal grid is constructed using the GridBuilder software [4]. The model has 290 grid cells in the east-west direction and 145 grid cells in the north-south direction yielding a resolution of approximately  $\Delta x, \Delta y = 2$  km in the horizontal directions. The model has 15 terrain-following depth levels which grow increasingly coarse towards the bottom. Model bathymetry is taken from a NOAA website (<https://www.ngdc.noaa.gov/mgg/greatlakes/>). The water is 4 °C throughout the water column. The model includes  $f$ -plane rotation of the Earth and is run for approximately 170 hours in model time.

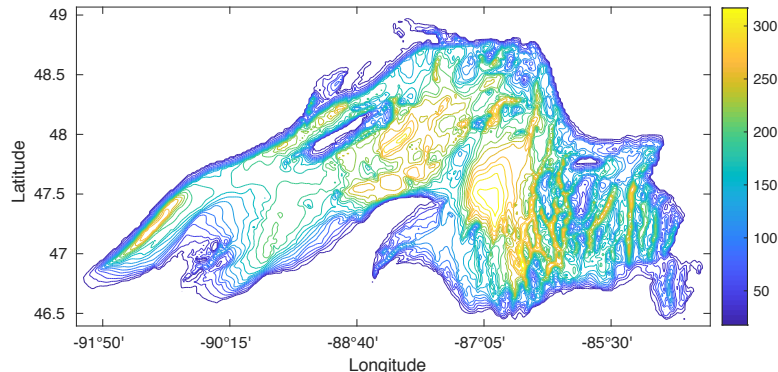


Figure 3.1: Model bathymetry in meters

The KPP mixing scheme simulates exchange of momentum by eddies in the vertical direction. A background vertical eddy viscosity of  $1 \times 10^{-5} \text{ m}^2\text{s}^{-1}$  is used. A value of  $5 \text{ m}^2\text{s}^{-1}$  was chosen for the horizontal viscosity coefficient. The model employs a linear bottom drag with an  $r$  value of  $5 \times 10^{-4} \text{ m s}^{-1}$  once again.

To begin to simulate the plumes, wind is blown from the northeast over the entire grid. The magnitude of the northeast wind stress is varied from  $0.05$ - $0.3 \text{ Nm}^{-2}$ . The wind's direction is selected so that it applies a stress down the axis of the southwestern portion of Lake Superior (Figure 3.2). This part of the lake will be referred to as the 'western arm' going forward.

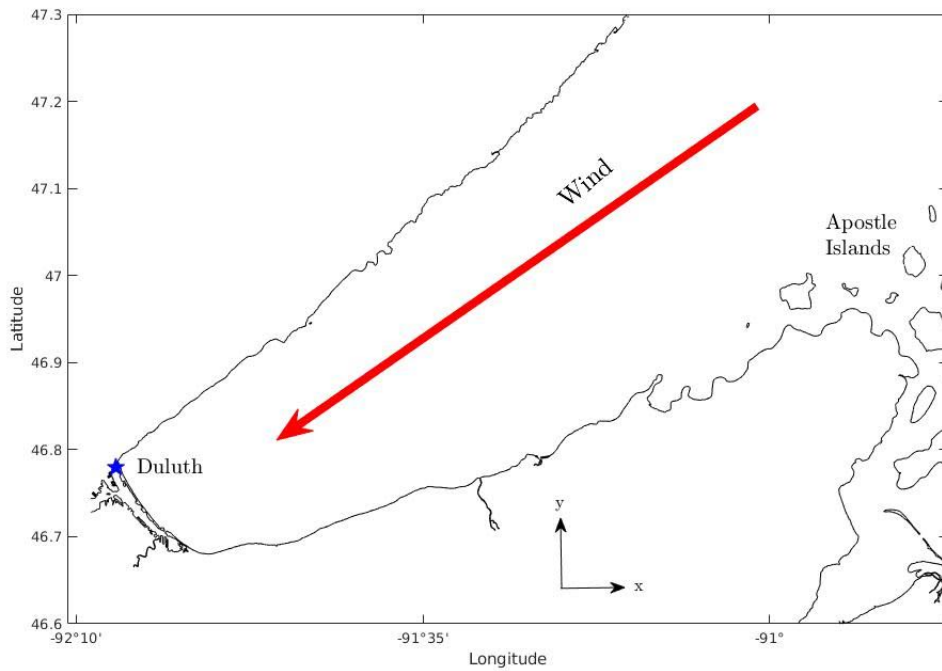


Figure 3.2: Northeast winds blowing down the western arm of Lake Superior

The velocities at each grid cell are vertically integrated so transports are worked with. The transports are studied along a transect that passes through the western arm. Like the idealized model, the transports are primarily in the direction of and opposite to the wind stress (Figure 3.3).

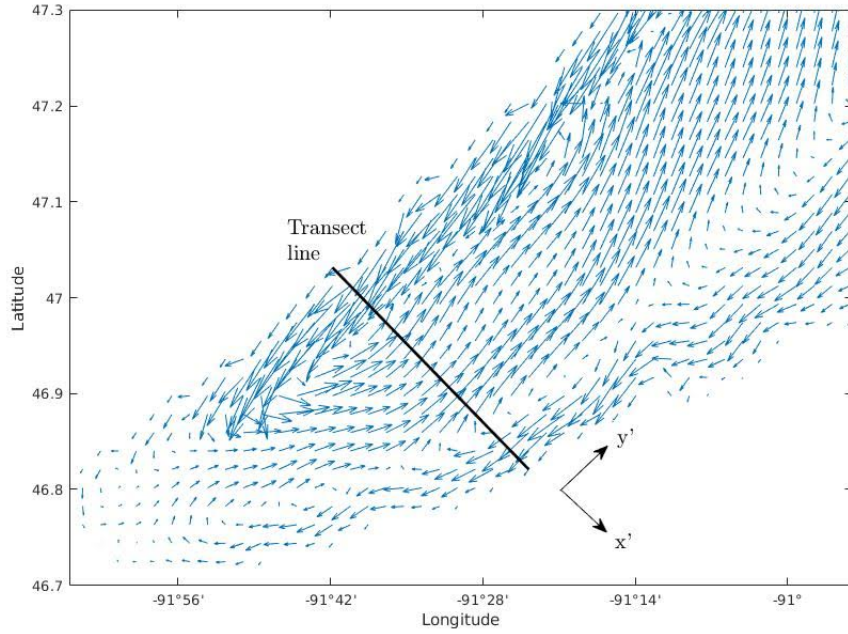


Figure 3.3: Transports are investigated along the transect and measured along the new axes

$q$  is calculated using the transport and stream function methods introduced earlier. The coordinate axes are rotated so that the component of the flow that is perpendicular to the transect line can be measured. The transport components after rotation of the coordinate axes are

$$\begin{bmatrix} U' \\ V' \end{bmatrix} = \begin{bmatrix} \cos\theta & \sin\theta \\ -\sin\theta & \cos\theta \end{bmatrix} \begin{bmatrix} U \\ V \end{bmatrix} \quad (3.1)$$

where  $U'$  is along the transect line,  $V'$  is perpendicular to it, and  $\theta$  is the angle the axes are rotated by. The perpendicular components moving opposite the wind stress are multiplied by the distance between grid cells and added up. This sum gives the transport method's estimate of  $q$ . This is completed for each model output time so that a time series of  $q$  is obtained.

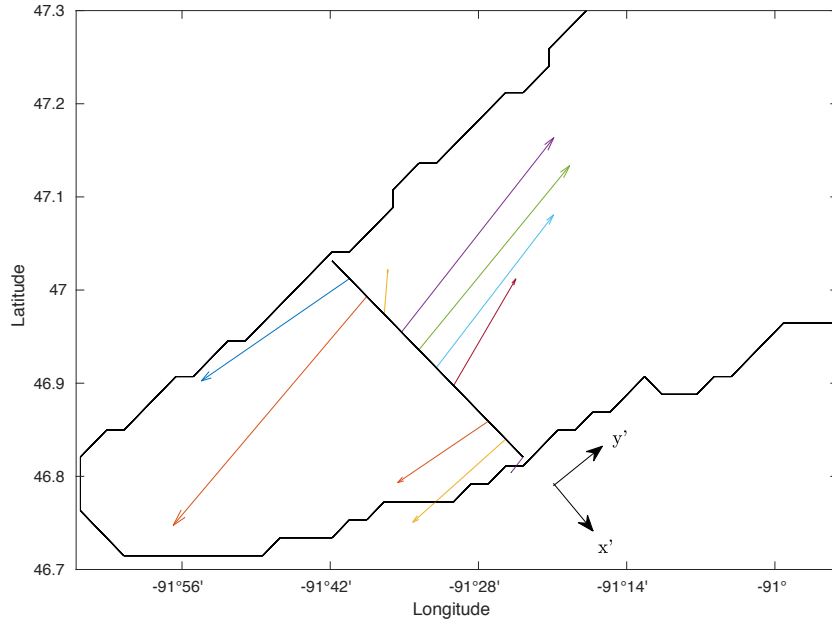


Figure 3.4: Transports are evaluated on the transect line

The stream function method begins by integrating one of the transport fields by Equation 2.15 to find  $\psi$  at each grid point (Figure 3.5). The grid cells where the velocities switch from being in the direction of the wind stress (coastal jets) to having direction opposite to the wind stress (return flow) are located and serve as the two locations to take a difference in  $\psi$ . This gives the stream function estimate of  $q$ .

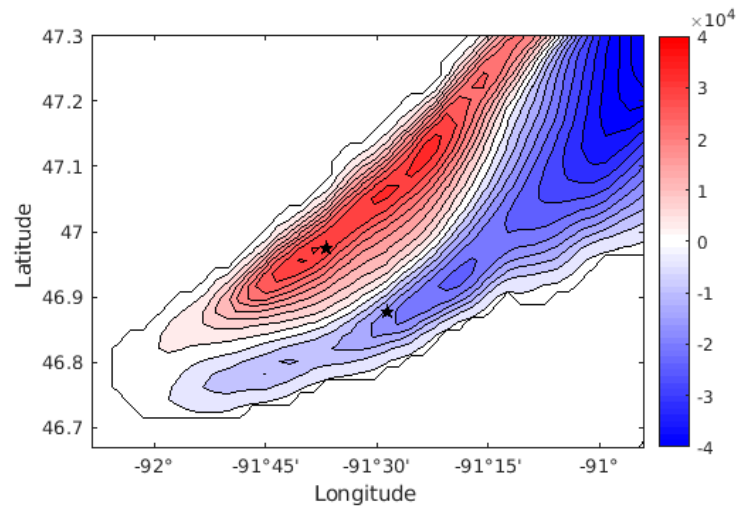


Figure 3.5: Selection of the zero-crossing points (black stars) in the transport stream-function field. Units on the colorbar are  $\text{m}^3\text{s}^{-1}$ .

Estimates of the flow rate made by the analytical, transport, and stream function methods are integrated in time from the start of steady-state to the end of the model run to obtain  $Q$  and then compared to one another.

---

## 3.1 Additional Tests

### 3.1.1 Surface Slope Analysis

Wind blowing down the axis of the western arm results in water being piled up on the arm's southwestern coast. The surge along the coast can be measured as the model outputs values for the surface elevation of the water above a reference height,  $\eta$ , for each grid cell. Two points that are found along the axis of the western arm and on opposite ends of the lake are chosen for  $\eta$  measurements (Figure 3.6).

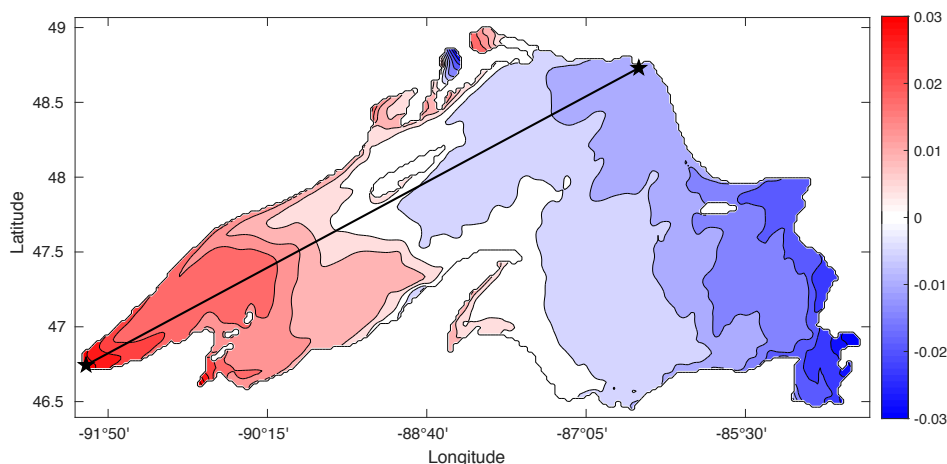


Figure 3.6: Points on the grid chosen for  $\eta$  measurements are marked by black stars. They are approximately 460 km apart. Plotted field is  $\eta$  and colorbar has units of meters

The two points are used to measure the slope of the surface elevation across the lake and how it varies with northeast wind stress.

### 3.1.2 Realistic Winds and Dye

A model with realistic winds from the April 23-29, 2016 storm was developed. The model is forced using wind speed and wind direction data that was taken from the National Data Buoy Center website for station DULM5. Data was collected by the buoys every six minutes and missing data was filled using linear interpolation. Wind speed was converted to wind stress by using the USGS's air-sea toolbox where DULM5's station height is 13.2 m above sea level. Wind direction is recorded at the station as degrees from north so this angle is subtracted from  $90^\circ$  when input into the ROMS NetCDF file. The reason for this is because the coordinate system selected for the model would read a  $0^\circ$  wind as blowing from the east where the physical station records that as wind blowing from the north.

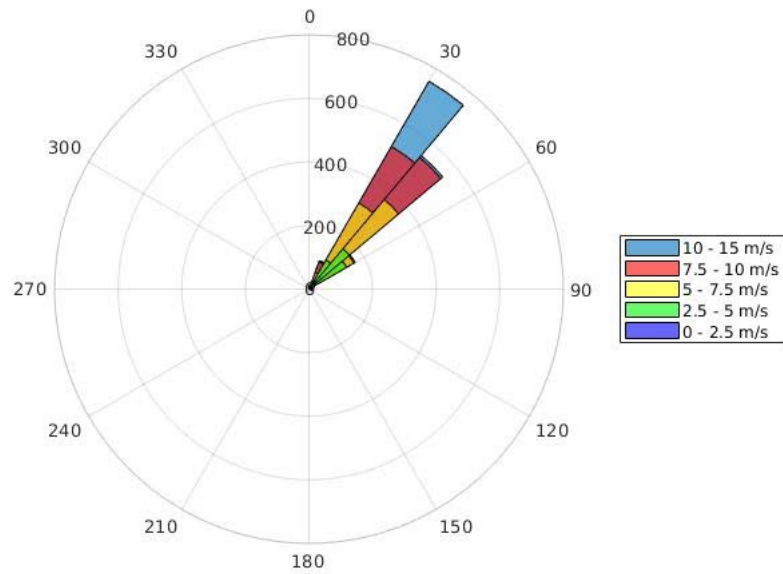


Figure 3.7: Wind direction and speed recorded by DULM5 for April 23-29, 2016. 0° would indicate a wind from the north

An attempt at modeling the sediment transport during the wind event is carried out in unison by inputting a tracer dye into the western arm through river point sources (Figure 3.8). One of the sources models the deposition of sediment into the western arm by the red clay banks of Wisconsin. The red clay banks of Wisconsin are assumed to be the primary source of sediment in the western arm plumes.

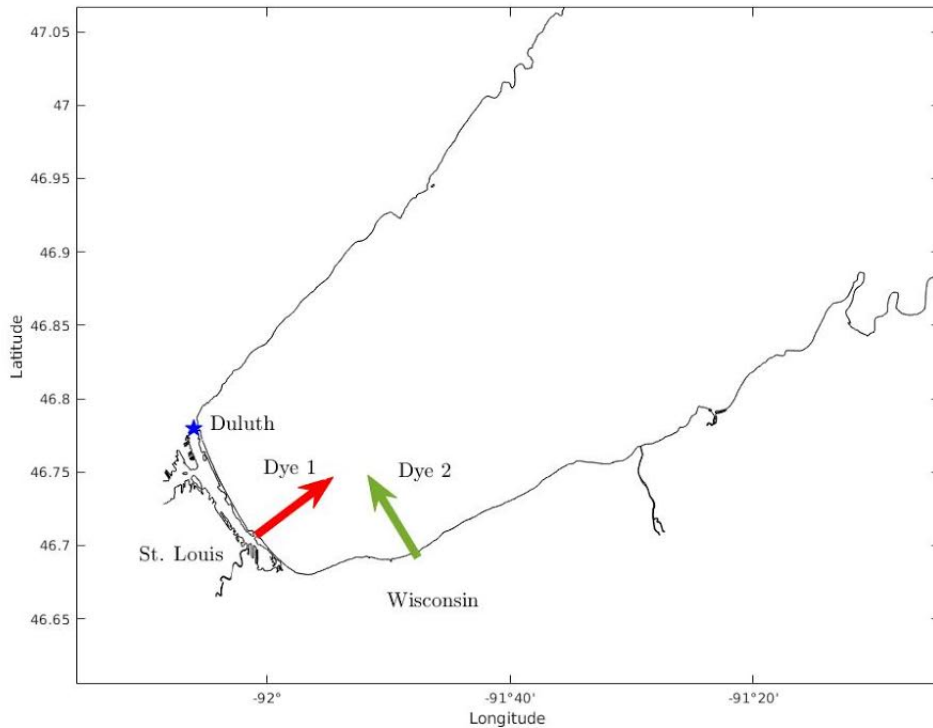


Figure 3.8: Approximate dye input points

The other source is modeled after the St. Louis river which is assumed to play an insignificant role in sediment deposition into the western arm (Sydor (1979)). This dye source is still of interest because it is near where the plumes typically form in the western arm. Both river sources have a volume flux of  $40 \text{ m}^3\text{s}^{-1}$ , temperature of  $4^\circ \text{ C}$ , and input dye equally into all 15 vertical levels.

## 3.2 Results

Like the idealized model, the realistic model produces strong coastal jets in shallower regions of the channel and a return flow in the deeper regions. The coastal current along the northern shore of the channel is considerably larger than the one on the southern shore. The coastal jets and return flow largely extend from the surface of the water column to the bottom (Figure 3.9). For the run forced by a  $0.1 \text{ Nm}^{-2}$  wind stress, the mean experimental return flow velocity was  $0.026 \text{ ms}^{-1}$  while the mean analytical velocity was  $0.062 \text{ ms}^{-1}$ .

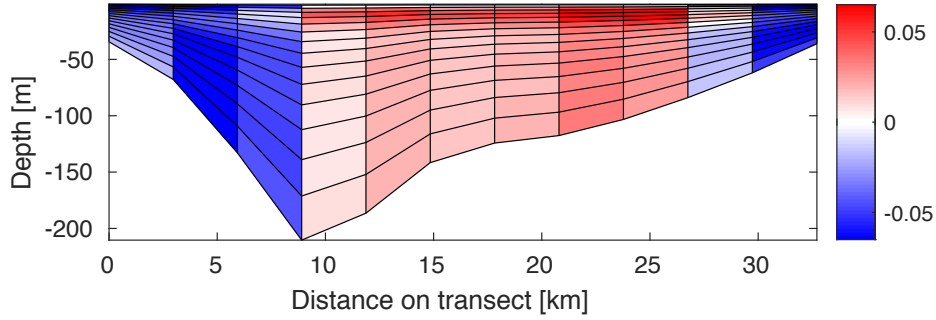


Figure 3.9: Vertical profile of along-channel velocity at transect. Colorbar has units of  $\text{ms}^{-1}$ .

The flow rate across the transect line in the southeastern portion of the lake was studied as the the northeast wind stress was varied. The flow rate is calculated using the transport method (Figure 3.10).

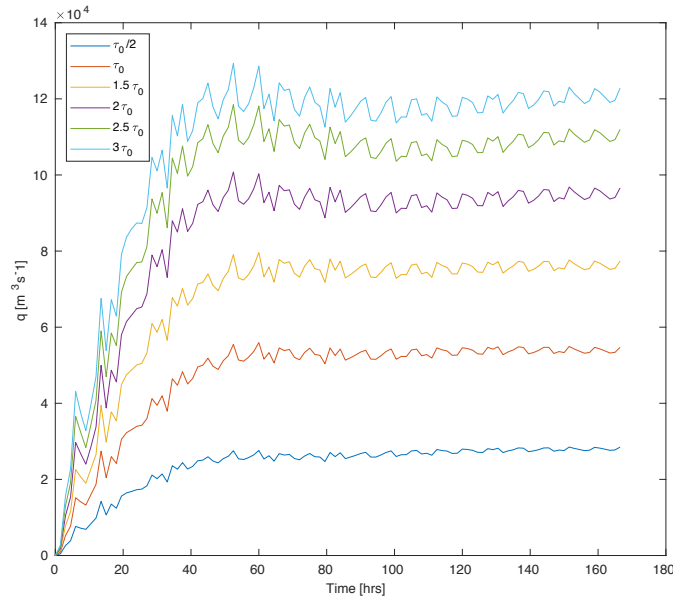


Figure 3.10: Time series of  $q$  calculated using the transport method. The northeast wind stress is varied.  $\tau_0 = 0.1 \text{ Nm}^{-2}$

Figure 3.10 shows that the  $q$  curves look similar to those seen for the idealized model. The steady-state value of  $q$  increases as the wind stress on the system does. Oscillations in  $q$  with a period of approximately 8 hours align with Lake Superior's surface seiche frequency [14].

Integrating the flow rates computed by the two experimental methods shows they make similar estimates of  $Q$  (Figure 3.11).

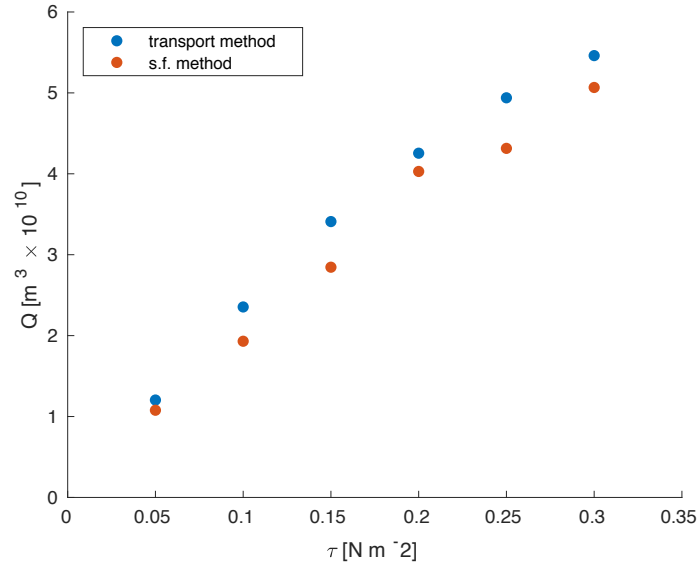


Figure 3.11: Experimental  $Q$  results using transport and stream function methods

In contrast to the idealized model, the modeled return flow rates were always smaller than the analytical predictions of those rates. This meant modeled offshore volume transport was smaller than analytical predictions as well (Figure 3.12).

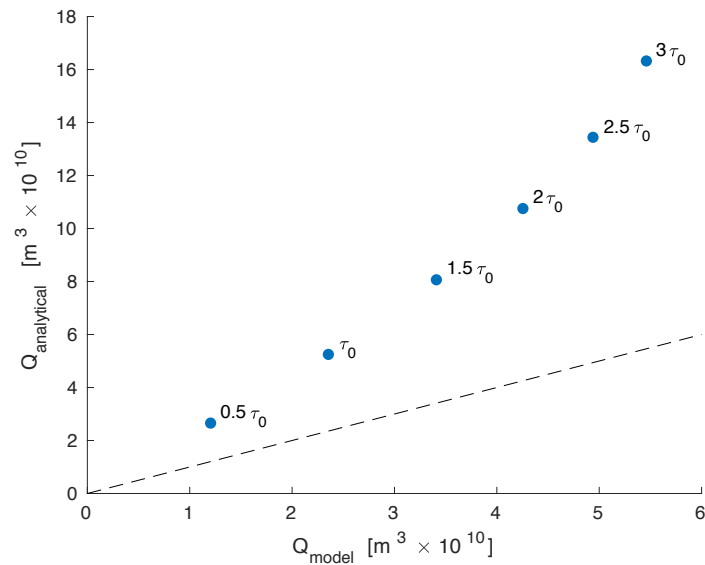


Figure 3.12: Experimental  $Q$  values are plotted against analytical  $Q$

Figure 3.12 shows that both experimental and analytical estimates of  $Q$  increase linearly with wind stress on the system and they are on the same order of magnitude at low wind stresses. Experimental  $Q$  increasing non-linearly beyond  $0.15 \text{ Nm}^{-2}$  suggests that non-linear processes in the channel become significant at higher wind stresses.

The surface slope of the lake was measured as the wind stress was varied (Figure 3.13). The setup at the southwestern end of the lake is also plotted.

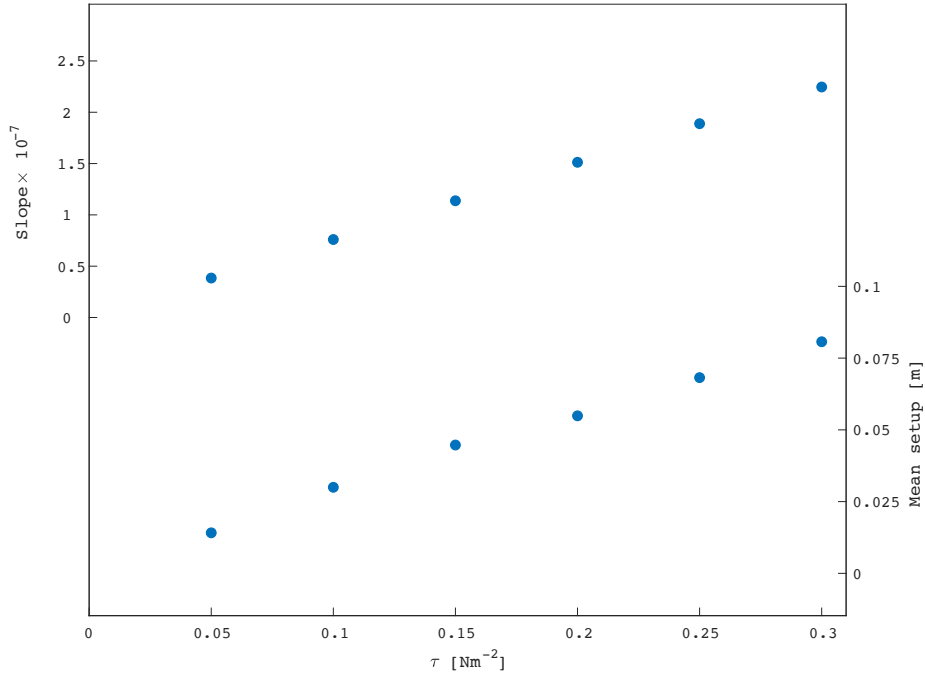


Figure 3.13: Slope of free surface between the points shown in Figure 3.6 and setup at southwestern coast of Lake Superior with varying wind stress

Figure 3.13 shows that the surface slope of the lake and setup along the southwestern coast of the lake change linearly with northeast wind stress. Lines of best fit yield the relationships  $\frac{d\eta}{dx} = 7.5 \times 10^{-7} [\frac{\text{m}^2}{\text{N}}] \tau$  and  $\bar{\eta} = 0.26 [\frac{\text{m}^3}{\text{N}}] \tau$  where  $\bar{\eta}$  is the mean surface elevation. The surface slope of the lake is less than idealized model's slope with the same wind stress. This is expected since, on average, Lake Superior is deeper than the idealized model and setup is greater for shallower lakes than deep ones.

Vertical integrals of dye concentration are plotted on April 27th, 2016 in model time for the model run with realistic winds. 10 contour levels of the dye concentration are plotted (Figure 3.14 and Figure 3.15).

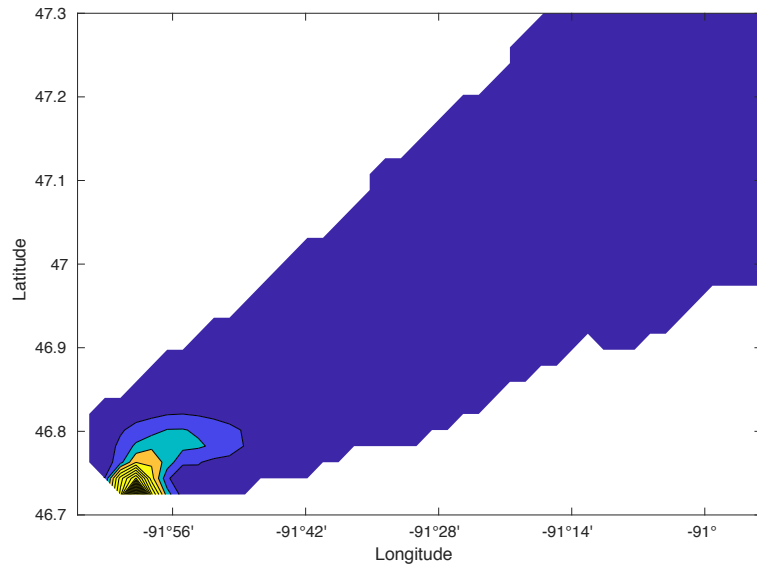


Figure 3.14: Vertically-integrated dye 1 concentration

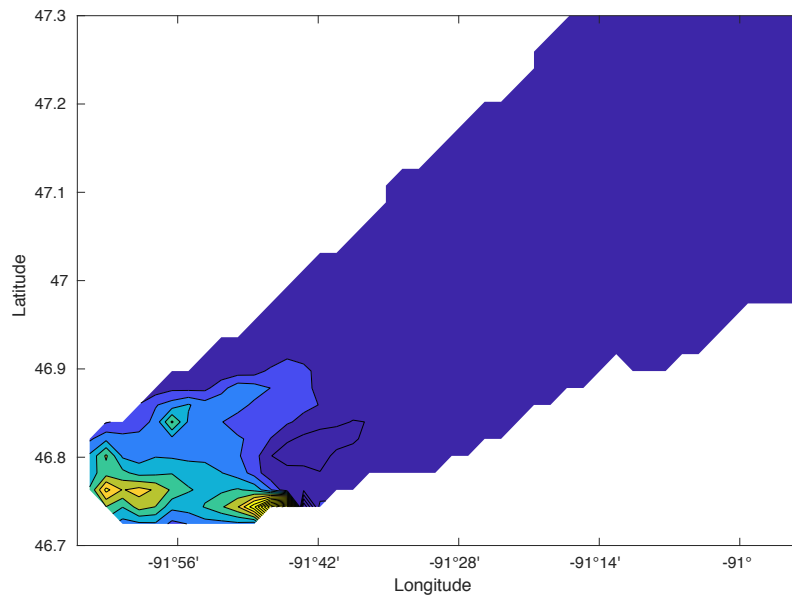


Figure 3.15: Vertically-integrated dye 2 concentration

Both Figure 3.14 and Figure 3.15 show that the released dye travels up the western arm with the return flow. In particular, dye 1 looks much like the observed sediment plume on April 27th, 2016.

### 3.3 Discussion

In this chapter, a realistic model of the circulation of wind-driven sediment plumes in Lake Superior was presented. The model produced the general features of the circulation, strong coastal currents moving in the direction of the wind stress and a

compensating return flow moving opposite the wind. The mean experimental flow rates were typically less than half those expected by the analytical approach. This resulted in experimental  $Q$  being half that of analytical  $Q$  at wind stresses below  $0.2 \text{ Nm}^{-2}$  and with the difference growing above it. Dye released in the western arm of Lake Superior during the model run with realistic winds gave a reassuring result. The dye traveled to the open lake with the return flow, much like the sediment in the observed plumes.

The slope analysis showed that the lake surface slope varied linearly with wind stress. Analytical and experimental surface slope were not compared like in the idealized model. Whereas one  $b$  value describes any transect for the idealized model, the bathymetry varies significantly for different transects in Lake Superior. Calculating the surface slope from one of these transects probably won't say much about the entire lake then. There was no atmospheric forcing in the model and if the surface elevation results were to be corroborated by field measurements this would have to be accounted for.

As mentioned above,  $b$  changes for different transects through the western arm. This means the analytical flow rate would change with different transects as well. Consequently, choosing a transect that is descriptive of the western arm as a whole is very important. To test that the chosen transect is reasonable, both analytical and experimental flow rates could be checked at other transects through the western arm to make sure the results don't change qualitatively.

Like the idealized model, the flow rates are likely dependent on choosing appropriate vertical mixing parameters and bottom drag coefficients. The KPP scheme outputs a vertical viscosity value of  $3.1 \times 10^{-3} \text{ m}^2\text{s}^{-1}$  across the entire grid for all model runs. Since the vertical viscosity was spatially variant in the idealized channel, it shows that the MITgcm and ROMS KPP schemes may differ. More attention will have to be paid to the bottom boundary layer (BBL) in future versions of the model. It was found late in the research process that the parameters dictating vertical layer thickness were not optimally chosen. The bottom most cells along the transect were often large ( $\approx 40 \text{ m}$ ) and a clear BBL wasn't visible in vertical profiles of along-channel velocity (Figure 3.16).

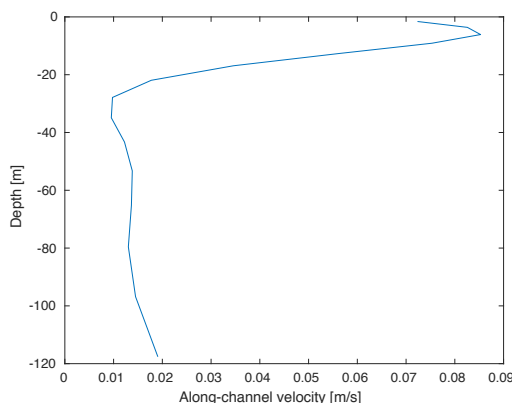


Figure 3.16: Vertical profile of along-channel velocity in return flow

Wind-driven sediment plumes in the Great Lakes are not restricted to Lake Superior. In the next chapter, a plume in Lake Huron is investigated.

# Chapter 4

## Realistic Model: Lake Huron

A second wind-driven sediment plume was observed in the Great Lakes during the late April 2016 wind event. The plume developed at the southeastern end of Lake Huron (Figure 4.1a) and provided another opportunity to compare the analytical approach to a realistic model of a lake's circulation. The model was developed and ran in ROMS to test the dependence of the plume's circulation on a wind from the north.

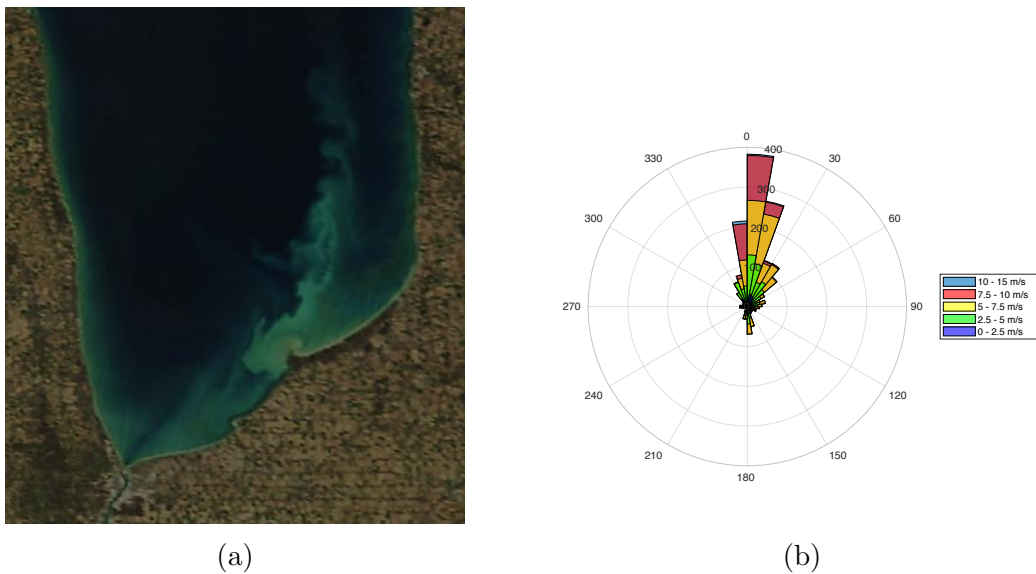


Figure 4.1: (a) Observed sediment plume in Lake Huron develops in the southeastern portion of the basin. (b) Wind data collected from weather station PSCM4 for dates plume was observed on (April 23-29, 2016). 0° indicates a wind that blows from the north.

The model grid has 200 cells in both the east-west and north-south directions yielding a grid resolution of approximately  $\Delta x, \Delta y = 2$  km in each direction. The model bathymetry is taken from the same NOAA database as the Lake Superior model (Figure 4.2).

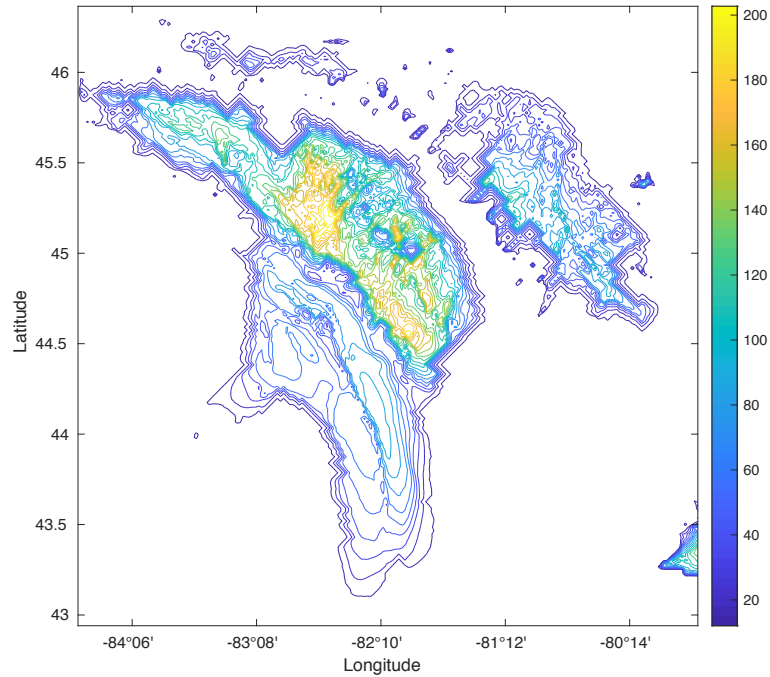


Figure 4.2: Model bathymetry in meters

The model uses the same parameters as the Lake Superior model including number of vertical levels, temperature profile, model run time, bottom drag, and sub-grid scale process schemes. The model is forced with wind stress magnitudes varying from  $0.1-0.3 \text{ Nm}^{-2}$ . The wind's direction is chosen so that it points down the channel in Lake Huron where the plume forms in (Figure 4.3).

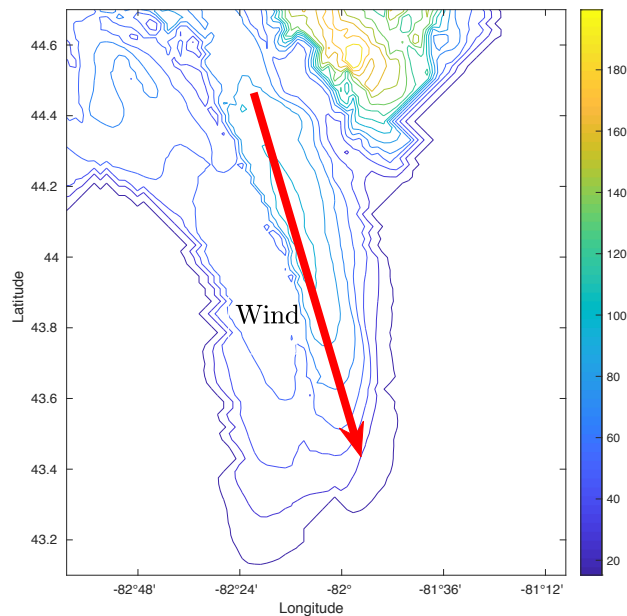


Figure 4.3: The model is forced by wind stress pointing down the southeastern basin

Transports are investigated along a transect line found in the southern end of the lake basin (Figure 4.4). No rotation of the coordinate axes is carried out since

the  $V$  transport field will be perpendicular to the chosen transect line. The value of  $q$  from the transport method will be compared to the analytical method.

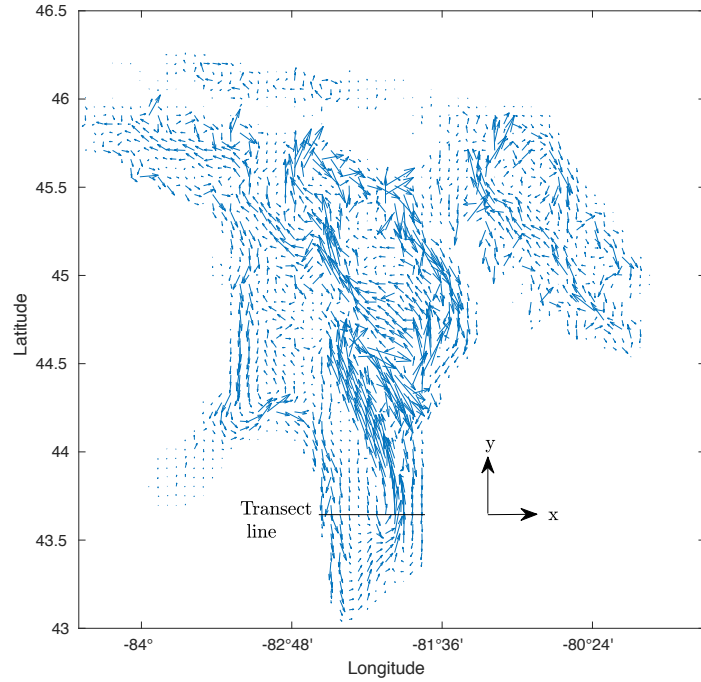


Figure 4.4: Transports are investigated along the transect line

## 4.1 Results

Once again, strong coastal currents develop in the shallower regions of the transect along with a compensating return flow in the deeper ones (Figure 4.5). The mean along-channel velocities are larger than those in the Lake Superior model with the same wind stress. The mean experimental return flow velocity was  $0.058 \text{ ms}^{-1}$  while the analytical mean velocity was  $0.031 \text{ ms}^{-1}$ .

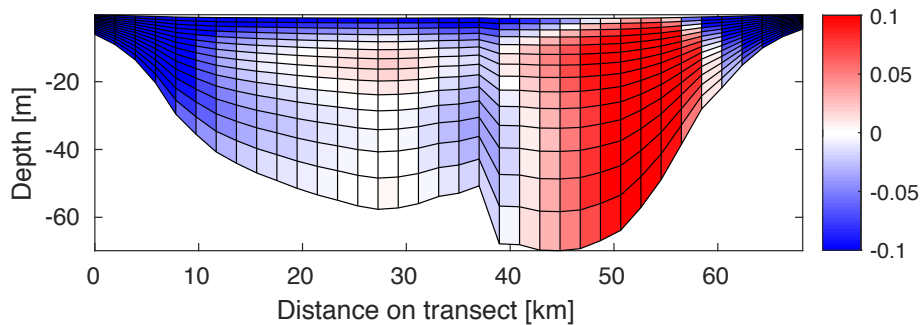


Figure 4.5: Along-channel velocities with depth on transect line. Units on the colorbar are  $\text{ms}^{-1}$ .  $\tau^{sfc} = 0.1 \text{ Nm}^{-2}$

The volume transport increased as the wind stress on the system did (Figure 4.6).

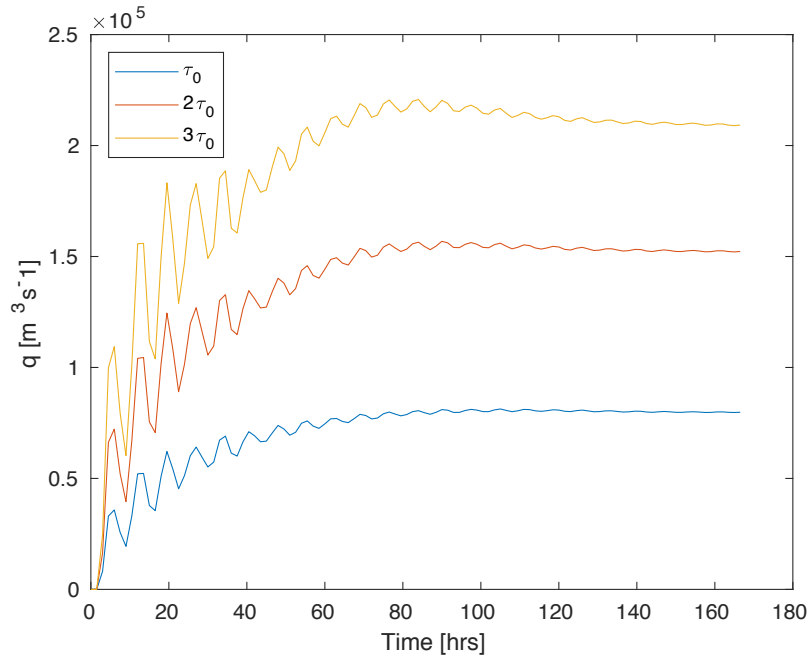


Figure 4.6: Time series of  $q$  calculated using the transport method with varying wind stress.  $\tau_0 = 0.1 \text{ Nm}^{-2}$

Figure 4.6 shows the time series of  $q$  have profiles that look like the Lake Superior ones but their steady-state values are considerably larger. A surface seiche frequency of approximately 7 hours aligns with estimates of Lake Huron’s lengthwise seiche frequency [18].

Modeled along-channel velocities being greater than analytical estimates resulted in modeled  $Q$  always being larger than analytical  $Q$  (Figure 4.7).

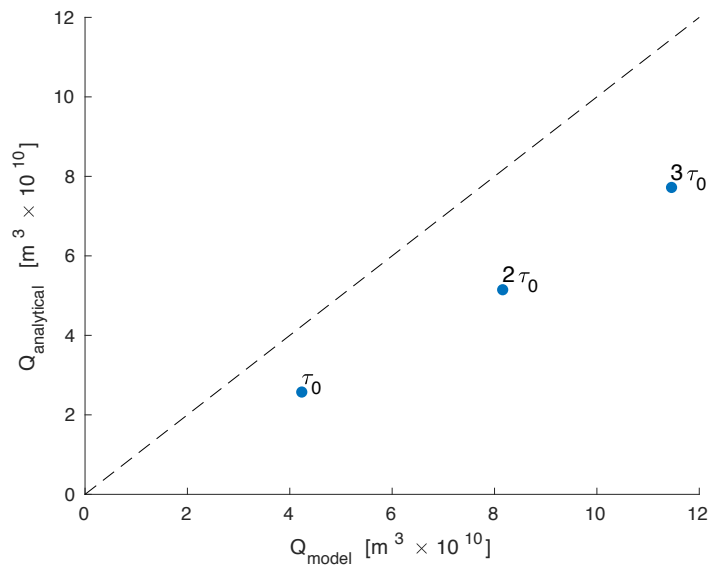


Figure 4.7: Comparison of  $Q$  for the three methods

Other takeaways from Figure 4.7 are that experimental and analytical  $Q$  were on the same order of magnitude and experimental  $Q$  varied linearly with wind stress

---

for the Lake Huron model.

## 4.2 Discussion

In this chapter, a realistic model of the circulation that produces a wind-driven sediment plume in Lake Huron was studied. We saw that the modeled along-channel velocities were greater than the modeled Lake Superior ones for the same wind stress. The experimental return flow velocities were also larger than the analytical estimates for the basin. Experimental  $Q$  was always larger than analytical  $Q$  as a result but the two were still on the same order of magnitude. Unlike the Lake Superior model,  $Q$  varied linearly with wind stress on the system all the way up to  $0.3 \text{ Nm}^{-2}$ . The results obtained with the chosen transect should be double-checked by investigating both analytical and experimental flow rates at other transects in southern Lake Huron.

As mentioned earlier,  $q$  will be dependent on the selection of the vertical mixing scheme and the bottom drag. The KPP algorithm uses the same vertical viscosity value as the Lake Superior model for all of the runs. A clearer BBL does develop along the transect since it's relatively shallow and the bottom most cells are smaller than in the Lake Superior model (Figure 4.8). The larger presence of the BBL could be why  $Q$  varied linearly with all wind stresses in this model and not in the Lake Superior one. It is likely that a BBL still does not form in the deeper portions of the Huron model.

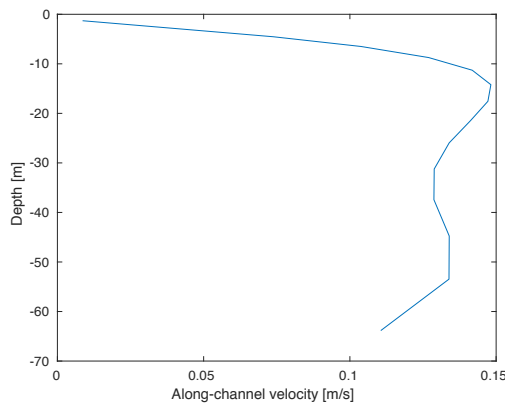


Figure 4.8: Vertical profile of along-channel velocity in return flow

Some interesting parallels between the idealized and Lake Huron models are the max depth along their transect and experimental  $Q$ . Both models have a max depth along their transect of under 100 m and an experimental  $Q$  that's always larger than the analytical estimate. The Lake Superior model has a max depth of approximately 200 m and had an experimental  $Q$  that was always smaller than analytical estimates. This may suggest that whether the analytical approach over or underestimates  $Q$  is dependent on the relationship between the typical depth of the transect and how well momentum is mixed throughout the water column. One test that could support this idea would be measuring  $Q$  for an idealized model that had the same average transect depth as the Lake Superior model. Other tests could include measuring  $Q$  as the depths of the realistic models are varied.

# Chapter 5

## Conclusion

This research shows that despite the simplifications made by the analytical approach, it makes estimates of  $Q$  that are on the same order of magnitude as idealized and realistic models. Like the analytical approach, the volume of water moved offshore in the models was typically linearly related to wind stress on the system and the basin's morphology.

Future directions for this work could include carrying out an idealized model run with an average depth similar to the Lake Superior transect and seeing if experimental  $Q$  is less than the idealized prediction. Differences between the ROMS and MITgcm models could also be avoided by running the idealized tests in the ROMS model. This would allow for more concrete comparisons between idealized and realistic circulations.

### 5.1 Significance to Society

McKinney et al. (2019) have shown that coastal waters are transported offshore during wind-driven plume events. This is of importance due to coastal waters having higher concentrations of biological and chemical constituents than waters in the open-lake. It was also shown in their paper that the amounts of coastal water transported offshore from year-to-year in these events varies significantly. This could play a role in ecological variability of Lake Superior. This work showed there was variability in offshore transport between lakes as well. For the same wind stress, the Lake Huron plume transported approximately double the water as the Lake Superior plume. This could lead to yearly ecological variability between the Great Lakes. Coastal waters are also home to pollutants that may have been deposited there from coastal runoff, river inputs, and industrial sources. In the event of a wind-driven plume, these pollutants may be relocated to the lake interior faster than if they had traveled with the lake's general circulation and may make remediation of coastal pollutants more difficult.

It is possible that the plumes develop near locations which are densely populated. This is the case for the plumes that develop in Lake Superior and Lake Michigan. The coastal communities near the Lake Superior plume make up approximately 45% of the lake's watershed population and the plume in Lake Michigan forms near Chicago which has a population of roughly 2.5 million. A deeper understanding of the ecology of the plume-impacted waters may benefit local industries like fishing if

---

correlations can be drawn between plume frequency and lake productivity.

This project naturally lent itself to the study of storm surge on Lake Superior with wind stresses over the lake changing the surface elevation of the water. Storm surge affects coastal communities worldwide, resulting in loss of life and significant infrastructure damage [13]. The communities of Duluth, MN and Superior, WI may benefit from an understanding of the relationship between storm surge and northeast wind stress as they routinely incur infrastructure damage due to storms involving storm surge as wind blows from the northeast.

# Chapter 6

## Bibliography

- [1] BEARDSLEY, R. C., MOFJELD, H., WIMBUSH, M., FLAGG, C. N., AND VERMERSCH JR., J. A. Ocean tides and weather-induced bottom pressure fluctuations in the middle-atlantic bight. *Journal of Geophysical Research (1896-1977)* 82, 21 (1977), 3175–3182.
- [2] BRINK, K. Cross-shelf exchange. *Annual Review of Marine Science* 8, 1 (2016), 59–78. PMID: 26747520.
- [3] CSANADY, G. T. Wind-induced barotropic motions in long lakes. *Journal of Physical Oceanography* 3, 4 (1973), 429–438.
- [4] DENHAM, C. R. Gridbuilder. ”<https://austides.com/wp-content/uploads/GridBuilder-v0.99.pdf>”.
- [5] EADIE, B. J., SCHWAB, D. J., ASSEL, R. A., HAWLEY, N., LANSING, M. B., MILLER, G. S., MOREHEAD, N. R., ROBBINS, J. A., VAN HOOFF, P. L., LESHKEVICH, G. A., LESHKEVICH, G. A., JOHNGEN, T. H., LAVRENTYEV, P., AND HOLLAND, R. E. Development of recurrent coastal plume in lake michigan observed for first time. *Eos, Transactions American Geophysical Union* 77, 35 (1996), 337–338.
- [6] GRIFFIN, D. A., AND MIDDLETON, J. H. Steady wind-driven flow in long channels or lakes. *Continental Shelf Research* 7, 9 (1987), 987 – 1000.
- [7] HALFMAN, B. M. H., AND JOHNSON, T. C. Surface and benthic nepheloid layers in the western arm of lake superior, 1983. *Journal of Great Lakes Research*” 15, 1 (1989), 15 – 25.
- [8] LOHRENZ, S. E., FAHNENSTIEL, G. L., MILLIE, D. F., SCHOFIELD, O. M. E., JOHNGEN, T., AND BERGMANN, T. Spring phytoplankton photosynthesis, growth, and primary production and relationships to a recurrent coastal sediment plume and river inputs in southeastern lake michigan. *Journal of Geophysical Research: Oceans* 109, C10.
- [9] MCKINNEY, P., AUSTIN, J., AND FAI, G. The wind-driven formation of cross-shelf sediment plumes in a large lake. *Limnology and Oceanography* 0, 0.
- [10] MEI, C. C. Notes on advanced environmental fluid mechanics. [http://web.mit.edu/fluids-modules/www/coastal\\_gfd/7-3-shallowwat.pdf](http://web.mit.edu/fluids-modules/www/coastal_gfd/7-3-shallowwat.pdf), 2002.

- 
- [11] MIT. Mitgcm: About. <http://mitgcm.org/about-mitgcm/>.
- [12] NOAA, N. C. F. E. I. Great lakes bathymetry. <https://www.ngdc.noaa.gov/mgg/greatlakes/>.
- [13] NOAA, N. H. C. Storm surge overview. <https://www.nhc.noaa.gov/surge/>.
- [14] RAO, D., AND SCHWAB, D. *Two-Dimensional Normal Modes In Arbitrary Enclosed Basins On A Rotating Earth: Application to Lakes Ontario and Superior*. Center for Great Lakes Studies, The University of Wisconsin–Milwaukee.
- [15] RAO, D. B., AND MURTY, T. S. Calculation of the steady state wind-driven circulations in lake ontario. *Archiv für Meteorologie, Geophysik und Bioklimatologie, Serie A 19*, 2 (Jun 1970), 195–210.
- [16] SCIENCE, S., AND ENGINEERING CENTER, U.-M. Modis today – cimss/ssec. <http://ge.ssec.wisc.edu/modis-today/>. [Online; accessed 14-March-2018].
- [17] SYDOR, M. *Red clay turbidity and its transport in Lake Superior*. Great Lakes National Program Office, US Environmental Protection Agency, Region V.
- [18] TREBITZ, A. S. Characterizing seiche and tide-driven daily water level fluctuations affecting coastal ecosystems of the great lakes. *Journal of Great Lakes Research 32* (2006).
- [19] YERUBANDI R. RAO, D. J. S. Transport and mixing between the coastal and offshore waters in the great lakes: a review. *Journal of Great Lakes Research 33*, 1 (2007), 202 – 218 – 17.